2516–2527 *Nucleic Acids Research, 2006, Vol. 34, No. 9*
doi:10.1093/nar/gkl221

The initial step of DNA hairpin folding: a kinetic analysis using fluorescence correlation spectroscopy

Jiho Kim, Sören Doose*, Hannes Neuweiler and Markus Sauer*

Applied Laser Physics and Laser Spectroscopy, University of Bielefeld, Universitätsstrasse 25, 33615 Bielefeld, Germany

Received February 14, 2006; Revised March 3, 2006; Accepted March 27, 2006

ABSTRACT

Conformational fluctuations of single-stranded DNA (ssDNA) oligonucleotides were studied in aqueous solution by monitoring contact-induced fluorescence quenching of the oxazine fluorophore MR121 by intrinsic guanosine residues (dG). We applied fluorescence correlation spectroscopy as well as steady-state and time-resolved fluorescence spectroscopy to analyze kinetics of DNA hairpin folding. We first characterized the reporter system by investigating bimolecular quenching interactions between MR121 and guanosine monophosphate in aqueous solution estimating rate constants, efficiency and stability for formation of quenched complexes. We then studied the kinetics of complex formation between MR121 and dG residues site-specifically incorporated in DNA hairpins. To uncover the initial steps of DNA hairpin folding we investigated complex formation in ssDNA carrying one or two complementary base pairs (dC–dG pairs) that could hybridize to form a short stem. Our data show that incorporation of a single dC–dG pair leads to non-exponential decays for opening and closing kinetics and reduces rate constants by one to two orders of magnitude. We found positive activation enthalpies independent of the number of dC–dG pairs. These results imply that the rate limiting step of DNA hairpin folding is not determined by loop dynamics, or by mismatches in the stem, but rather by interactions between stem and loop nucleotides.

INTRODUCTION

The hairpin-loop is a structural element that is present in DNA and RNA molecules *in vivo* as well as *in vitro* systems. It is known to play a key role in biological functions such as regulation of gene expression and facilitation of mutagenic events (1,2). DNA hairpins have also been used as highly sensitive reporters, so-called molecular beacons, for *in vitro* assays (3–5), and serve as model systems for secondary structure formation in DNA and RNA (6–8).

Individual hairpins fluctuate between different conformations that are often grouped into an open and a closed state. The thermodynamics and kinetics of DNA hairpins have been extensively studied using NMR, biochemical and spectroscopic methods (9–20). However, mostly hairpin structures with a stem of five or more complementary base pairs have been investigated. Only few reports examined thermodynamics of hairpin-loops with shorter stems (21,22). Kinetic studies of DNA hairpins were carried out, e.g. by Libchaber and co-workers (23,24) who examined DNA hairpin-loop formation monitoring fluorescence quenching using fluorescence correlation spectroscopy (FCS) and found that rates for loop formation depend on the loop sequence and length. Ansari and co-workers (6,25–28) confirmed these results using the laser temperature jump (T-jump) method and determined a length dependence that was in agreement with a semiflexible polymer model. Klenerman and co-workers (29–31) found a deviation from pure exponential kinetics when monitoring Förster resonance energy transfer (FRET) fluctuations in donor-acceptor labeled DNA hairpins. It has been proposed that the opening process depends on the unzipping energy of the hairpin, while the closing process relies on the collision of the two stalks of the stem, successive nucleation and propagation of base-pairing (25).

*To whom correspondence should be addressed. Tel: +49 521 106 5440; Fax: +49 521 106 2958; Email: sdoose@physik.uni-bielefeld.de
*Correspondence may also be addressed to Markus Sauer. Tel: +49 521 106 5450; Fax: +49 521 106 2958; Email: sauer@physik.uni-bielefeld.de
Present address:
Jiho Kim, Institut Pasteur of Korea, 39-1, Hawolgok-dong, Seongbuk-gu, Seoul 136-791, Korea

The authors wish it to be known that, in their opinion, the first two authors should be regarded as joint First Authors

Interestingly, some controversy exists over activation energies for DNA hairpin closing. While Goddard *et al*. (24) reported positive activation energies from kinetic measurements, Ansari *et al*. (25) and Wallace *et al*. (29) reported negative activation energies for very similar hairpin sequences. In fact Wallace *et al*. found clear deviations from Arrhenius kinetics for both opening and closing of hairpin-loops that was later confirmed by Ansari and co-workers. Ansari and co-workers (28) suggested an influence of misfolded states and proposed a model combining semiflexible polymer properties with a nucleation-zipping mechanism for hairpin closing. A recent suggestion for the origin of these discrepancies is based on observations of a three state folding pathway by Jung and VanOrden (8). They resolved a difference between the equilibrium constant measured by either ensemble steady-state fluorescence or FCS, which could have resulted in incorrect deviations of rate constants. Also, the dependence of closing and opening rates on the stem length has not been thoroughly studied and is still unknown. These unresolved questions provide the starting point for our studies.

Here, we investigate conformational dynamics of hairpin-forming single-stranded DNA (ssDNA). The DNA sequences consist of 3–9 loop nucleotides (thymines, dT), enclosed on both ends by 0–2 complementary nucleotides (cytosine, dC, and guanosine, dG) that can hybridize and form a short stem: MR121–5′-$(dC)_y$–$(dT)_x$–$(dG)_y$-3′ end ($x = 3$, 4, 5, 6 and 9; $y =$ 0, 1 and 2). MR121 is an oxazine fluorophore that serves as reporter for conformational changes by interacting with guanosine (32,33).

The fluorescence of oxazine and rhodamine fluorophores is known to be quenched selectively upon complex formation with dG or tryptophan due to photoinduced electron transfer (PET) (33–37). This PET-based quenching mechanism lays the foundation for a single-molecule sensitive tool, which allows probing conformational changes in macromolecules through a reporter fluorophore that is in a fluorescent or non-fluorescent state depending on the proximity of dG. Complex formation between a fluorophore that is site-specifically incorporated into an oligonucleotide and intrinsic dG can be observed with high sensitivity and nanosecond time resolution and report on conformational dynamics (32,38). Furthermore, selective fluorescence quenching can be used advantageously in the design of molecular beacons (or smart probes) to detect specific DNA sequences in fluorescence assays by a fluorescence increase upon hybridization to complementary target sequences (33,39,40).

In contrast to FRET-based systems that depend on long-range dipole–dipole interactions, PET-based quenching occurs only when fluorophore and dG are at van der Waals contact. Also the system's two-state nature (quenched/non-quenched fluorescence) without intermediate intensity values simplifies data analysis and in particular allows straightforward interpretation of correlation analysis. In fact FCS has become an established tool to monitor the conformational dynamics of flexible biopolymers, providing rate constants directly through amplitudes and characteristic decay times of FCS curves (23,24,29,37,38,41–44). It allows one to analyze diffusion constants, photophysical parameters and fluctuations in FRET or PET, and has been applied successfully to a wide number of molecular systems (45).

In order to accurately estimate closing and opening rate constants we first characterize intermolecular quenching interactions between MR121 and guanosine monophosphate (dGMP). Our data demonstrate that efficient quenching occurs in complexes on time scales below 50 ps, presumably due to PET from the ground state of the guanine moiety to the first excited singlet state of the fluorophore. In agreement with steady-state fluorescence experiments, FCS reveals the formation of non-fluorescent complexes that last for nearly hundred nanoseconds at room temperature. We estimate the efficiency of complex formation upon contact between dGMP and MR121, the time until dissociation occurs, and the associated binding energy.

The obtained results are essential for the interpretation of FCS data recorded for the various hairpin samples. We find that attachment of complementary nucleotides at the end of the DNA induces the formation of a stem that dramatically influences both opening and closing rate constants. Whereas the kinetics of homopolymers without stem-forming nucleotides could be well fitted using a monoexponential function, the incorporation of as little as one complementary base pair (dC–dG pair) alters the correlation decay to be multiexponential, revealing deviation from two-state kinetics. We present a thorough analysis of rate constant and activation enthalpy dependences on loop and stem length.

MATERIALS AND METHODS

Materials

Synthetic oligonucleotide sequences were purchased from IBA (Göttingen, Germany). 2-Deoxyguanosine-5-monophosphate (dGMP) was purchased from Sigma (München, Germany). The fluorescent oxazine dye MR121 (32) was kindly provided by K. H. Drexhage (ATTO-TEC GmbH, Siegen, Germany). All measurements were performed in aqueous solution of phosphate-buffered saline (PBS), pH 7.4 (137 mM NaCl, 2.7 mM KCl; Sigma, München, Germany), containing 0.1 mM EDTA (Sigma), 0.05% Tween 20 (Sigma) and 0.3–1.0 mg/ml bovine serum albumin (Sigma) to prevent glass surface interactions.

Synthesis of ssDNA

We investigated DNA oligonucleotides that consist of a polythymine (dT) part (called loop) and the complementary nucleobases cytosine (dC) and guanosine (dG) on either side of the loop (called stem) that can hybridize to form a hairpin structure: 5′-$(dC)_y$–$(dT)_x$–$(dG)_y$-3′ with $x = 3$–9 and $y = 1$ and 2. The 5′ ends of DNA oligonucleotides were labeled with MR121 via an aliphatic amino modifier C_3 using classical N-hydroxysuccinimidylester (NHS-ester) chemistry. Labeling was performed in PBS buffer containing 10% (v/v) carbonate buffer (100 mM, pH 8.5). A 5-fold molar excess of NHS-ester was added to 15–20 nM oligonucleotide and incubated for 2 h at room temperature in the dark. Fluorescently modified oligonucleotides were purified using reversed-phase (Hypersil-ODS column) high-performance liquid chromatography (Agilent Technologies, Waldbronn, Germany). Separation was performed in 0.1 M triethylammonium acetate, using a linear gradient from 0 to 75% acetonitrile in 20 min.

Fluorescence measurements

Absorption measurements were recorded using an UV-Vis spectrometer (Lambda 25; Perkin Elmer, USA). Steady-state fluorescence spectra were measured at room temperature using a Cary Eclipse fluorescence spectrometer (Varian, Darmstadt, Germany). Fluorescence quantum yields of labeled oligonucleotides were determined with respect to the fluorescence intensity F_0 of reference oligonucleotides carrying no dG [MR121–$(dT)_4$]. Fluorescence lifetimes were measured by time-correlated single-photon counting (TCSPC) using a standard TCSPC spectrometer (model 5000MC; IBH, Glasgow, UK) equipped with a pulsed laser diode (635 nm) as excitation source. In order to exclude polarization effects, all measurements were performed under the magic angle (54.7°). The decay parameters were determined by least-square deconvolution, and their quality was judged by the reduced χ^2-values, and the randomness of the weighted residuals. In all cases a biexponential model was adequate to describe the measured decay as provided in the following equation:

$$I = I_0(a_1\tau_1 + a_2\tau_2), \quad \mathbf{1}$$

where a_i are pre-exponential factors that describe the ratio of the excited species and τ_i denote their lifetimes. Owing to the limited time resolution strongly quenched populations with decay times shorter than ~50 ps were not revealed. The steady-state and dynamic quantum yield were calculated from fluorescence intensity F and lifetime τ, respectively: $QY_{ss} = F/F_0$ and $QY_{dyn} = \tau/\tau_0$, where τ_0 and F_0 are the fluorescence lifetime and intensity of the reference dye (MR121) or oligonucleotide [MR121–$(dT)_4$]. QY_{ss} is the product of the static and dynamic quantum yield, $QY_{ss} = QY_{stat} \times QY_{dyn}$, where QY_{dyn} reflects collisional quenching and QY_{stat} reflects the formation of non-fluorescent complexes.

FCS measurements

FCS measurements were conducted on a standard inverse fluorescence microscope setup (Axiovert 100; Zeiss, Germany), equipped with a HeNe laser emitting at 632.8 nm as excitation source. The collimated laser beam was coupled into an oil-immersion objective (63×, NA 1.4; Zeiss, Germany) by a dichroic beam splitter (645DLRP; Omega Optics, Brattleboro, VT, USA). The average laser power was adjusted to be 500 μW before entering the aperture of the objective. The fluorescence signal was collected by the same objective, filtered by a band-pass filter (700DF75; Omega Optics; Brattleboro, VT, USA) and imaged onto the active area of avalanche photodiodes (APD, SPCM-AQR-14; EG&G, Canada) via multi-mode optical fibers with a core diameter of ~100 μm. Fluorescence photons were shared by two APDs using a non-polarizing cubic beam splitter in order to circumvent deadtime and afterpulsing effects. The signals of the two APDs were recorded in cross correlation mode (300 s for each measurement) using a hardware correlator device (ALV-6010; ALV-GmbH, Langen, Germany), yielding a maximum time resolution of 6.25 ns. Temperature was controlled by heating/cooling the objective with a custom-made water-cooling device. The premixed samples were transferred onto microscope slides with a small depression and covered by a cover slip. All FCS measurements were performed at sample concentrations on the order of 1 nM, a concentration at which intermolecular interactions are negligible.

FCS data analysis

Fluorescence fluctuations caused by diffusion of molecules through the excitation/detection volume could be described sufficiently well by a 2D-diffusion model.

$$G_D(\tau) = \frac{1}{N[1 + (\tau/\tau_D)]}, \quad \mathbf{2}$$

where N is the number of particles in the observation volume and τ_D is the characteristic diffusion time. Assuming an all-or-none transition between a fluorescent and non-fluorescent state, the correlation function can be described by the product of a monoexponential decay and the diffusion term (46):

$$G(\tau) = G_D(\tau)\left(1 + K\exp\left[-\left(\frac{\tau}{\tau_{rel}}\right)\right]\right), \quad \mathbf{3}$$

or a stretched-exponential form, when multiple overlapping relaxation kinetics contribute (47):

$$G(\tau) = G_D(\tau)\left(1 + K\exp\left[-\left(\frac{\tau}{\tau_{rel}}\right)^{\beta}\right]\right), \quad \mathbf{4}$$

where K is the equilibrium constant between open and closed state, and β is a stretch exponent. The mean relaxation times $\langle\tau_{rel}\rangle$ were calculated as follows.

$$\langle\tau_{rel}\rangle = \int_0^\infty \exp\left[-\left(\frac{t}{\tau_{rel}}\right)^{\beta}\right]dt = \left(\frac{\tau_{rel}}{\beta}\right)\Gamma(\beta^{-1}), \quad \mathbf{5}$$

where $\Gamma(\beta^{-1})$ is the gamma function (31). Using K and $\langle\tau_{rel}\rangle$, average closing and opening rate constants can be calculated as follows:

$$k_{cl} = \frac{K}{\langle\tau_{rel}\rangle(K+1)}, \quad k_{op} = \frac{1}{\langle\tau_{rel}\rangle(K+1)}. \quad \mathbf{6}$$

RESULTS

Bimolecular quenching interactions between MR121 and dGMP

We first studied intermolecular quenching interactions between freely diffusing molecules MR121 and dGMP, the reporting quencher pair. As the individual entities diffuse in buffered solution, bimolecular interactions are observed that result in fluorescence quenching and can be analyzed using steady-state and time-resolved fluorescence spectroscopy, as well as FCS.

Steady-state and time-resolved fluorescence spectroscopy. In aqueous solvents MR121 exhibits an absorption maximum at 661 nm, and emits with a fluorescence lifetime τ_0 of 1.85 ns at an emission maximum of 673 nm. For bimolecular fluorescence quenching studies, solutions containing MR121 (<1 μM) and various concentrations of dGMP (0–60 mM) were prepared in PBS (pH 7.4). Upon addition of dGMP the absorption maximum shifted up to ~5 nm towards the red. Fluorescence emission spectra revealed a small

bathochromic shift of ~1–2 nm and a substantial decrease in fluorescence intensity. At a dGMP concentration of 10 mM the initial steady-state fluorescence intensity F_0 of MR121 dropped to $F \approx 0.5F_0$ (Figure 1a). Time-resolved fluorescence decays exhibited biexponential behavior with a fast component τ_1 of 100–300 ps nearly independent of the quencher concentration (<20% relative amplitude) and a slower component τ_2 linearly dependent on the quencher concentration. The average fluorescence lifetime $\tau = \tau_1 a_1 + \tau_2 a_2$ of MR121 (a_1, a_2 are relative amplitudes of both components) decreased by only 10% at a dGMP concentration of 10 mM. Since only τ_2 is dependent on the quencher concentration it should reflect collisional quenching yielding a dynamic quantum yield of 0.96 at 10 mM dGMP.

Overall three quenching contributions could be identified: (i) dynamic quenching that originates from collisional encounters between electronically excited MR121 and dGMP reducing the fluorescence lifetime (reflected in the longer decay component τ_2); (ii) formation of weakly fluorescent ground state complexes with a fluorescence lifetime τ_1 of 100–300 ps; and (iii) static quenching that does not affect the lifetime but occurs as a result of formation of non-fluorescent MR121–dGMP complexes (32). Comparison of static and dynamic quantum yield allowed us to estimate that ~5–10% of all complexes show weak fluorescence probably due to unfavorable interaction geometry. Steady-state and lifetime measurements of MR121 as a function of dGMP concentration can be presented as Stern–Volmer plots (Figure 1a) and analyzed using the following equations.

$$\frac{F_0}{F} = (1 + k_d\tau_0[\mathrm{dGMP}])(1 + K_s[\mathrm{dGMP}]), \quad \mathbf{7}$$

and

$$\frac{\tau_0}{\tau} = (1 + k_d\tau_0[\mathrm{dGMP}]), \quad \mathbf{8}$$

where F_0 and τ_0 (F and τ) are fluorescence intensity and average lifetime in the absence (presence) of dGMP, k_d is the dynamic quenching rate constant, and K_s is the static quenching constant. From the longer fluorescence lifetime component we extracted a bimolecular dynamic quenching rate constant $k_d = (1.39 \pm 0.09) \times 10^9 \mathrm{s}^{-1}\mathrm{M}^{-1}$ and a bimolecular static quenching constant $K_s = 75 \pm 2\ \mathrm{M}^{-1}$.

With knowledge of the collision radii $R_{\mathrm{dGMP/MR121}}$ and diffusion constants $D_{\mathrm{dGMP/MR121}}$, the bimolecular dynamic rate constant can be compared with a theoretical

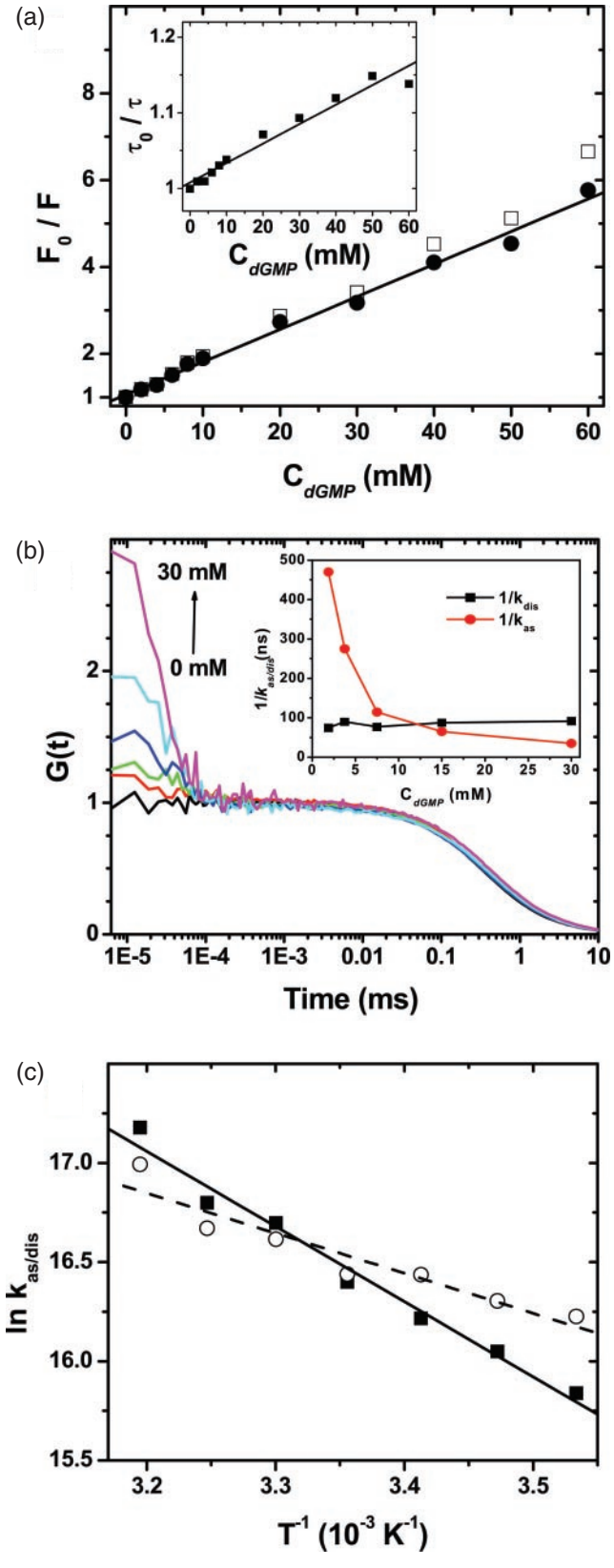

Figure 1. Bimolecular interaction between MR121 and guanosine. (**a**) Steady-state and time-resolved bimolecular Stern–Volmer plots of MR121 with dGMP in PBS, pH 7.4. F_0 (F) and τ_0 (τ) are the fluorescence intensity and longer lifetime component in the absence (presence) of dGMP. Squares represent the absolute intensity values F_0/F without any correction. Circles show static quenching, given by the quenching factor F_0/F divided by dynamic quenching $\tau_0/\tau = 1 + 2.6\mathrm{M}^{-1} \cdot [\mathrm{dGMP}]$ (as shown in inset). A linear fit of the static quenching curve yields the biomolecular association constant $K_s = 75 \pm 2\mathrm{M}^{-1}$. (**b**) Formation of non-fluorescent MR121–dGMP complexes monitored by FCS. FCS was performed at 20°C in aqueous solution of MR121 (~1 nM) and varying dGMP concentrations (0–30 mM). Association and dissociation rate constants $k_{\mathrm{as/dis}}$ were derived from parameters fitted according to Equation 3. The inset shows the variation of $\tau_{\mathrm{as/dis}} = k_{\mathrm{as/dis}}^{-1}$ as a function of dGMP concentration. (**c**) Arrhenius plots $\ln k_{\mathrm{as/dis}} = I - \Delta H(RT)^{-1}$ for the intermolecular interaction between MR121 and dGMP between 10 and 40°C. Closed squares (open circles) represent association (dissociation) rate constants. Arrhenius plots yield $\Delta H^{\mathrm{dis}} = 31 \pm 2$ kJ mol^{-1} and $\Delta H^{\mathrm{as}} = 17 \pm 2$ kJ mol^{-1}.

diffusion-limited bimolecular collision rate constant k_{col}, calculated from the Smoluchowski Equation (48):

$$k_{col} = \frac{4\pi N_A}{1000}(R_{dGMP} + R_{MR121})(D_{dGMP} + D_{MR121}), \quad \mathbf{9}$$

where N_A is the Avogadro number, and units for $R_{dGMP/MR121}$ and $D_{dGMP/MR121}$ are cm and $cm^2\ s^{-1}$, respectively. Assuming diffusion constants $D_{dGMP} = 5.0 \times 10^{-6} cm^2 s^{-1}$ (35) and $D_{MR121} = 2.8 \times 10^{-6} cm^2 s^{-1}$ [set equal to the diffusion constant of rhodamine 6G (41)], and a center-to-center distance between contact-forming MR121 and dGMP $R_{dGMP} + R_{MR121} = 0.7 \pm 0.3$ nm (estimated as the sum of van der Waals radii in different interaction geometries), we estimated a theoretical diffusion-limited bimolecular collision rate constant $k_{col} = (4.1 \pm 1.8) \times 10^9 s^{-1} M^{-1}$. Comparison with the experimentally observed bimolecular dynamic quenching rate constant $k_d = (1.39 \pm 0.09) \times 10^9 s^{-1} M^{-1}$ demonstrates that every second to third collision between dGMP and MR121 is effective in dynamically quenching the excited state.

Fluorescence correlation spectroscopy. To further investigate kinetics of complex formation we performed FCS measurements on mixtures of MR121 (~1 nM) and dGMP (0–30 mM). FCS allows direct monitoring of association/dissociation kinetics. Knowing that MR121 and dGMP form stable non-fluorescent complexes driven by hydrophobic interactions, we can assume an equilibrium between two states for the fluorophore: an on-state A (solvent-separated molecules) and an off-state B (non-fluorescent complex). Both states are populated according to association rate k_{as} and dissociation rate k_{dis}:

$$A \underset{k_{dis}}{\overset{k_{as}}{\rightleftharpoons}} B. \quad \mathbf{10}$$

Fluctuations of fluorescence intensity that arise from complex formation can then be analyzed by FCS using Equation 3. In this case, K corresponds to the equilibrium constant $K = [B]/[A] = k_{as}/k_{dis}$, and the exponential time constant τ_{rel} is the inverse sum of the association and dissociation rate constant of MR121 and dGMP, $\tau_{rel} = (k_{as} + k_{dis})^{-1}$.

FCS measurements were performed with an excitation power of <500 μW to minimize triplet state formation of the fluorophore. Figure 1b shows FCS correlation curves of MR121 in the presence of dGMP (0–30 mM) at 20°C. The data are in agreement with ensemble measurements by yielding an equilibrium constant close to 1 at a dGMP concentration of ~11 mM at 20°C.

We extracted association and dissociation rate constants from K and τ_{rel} according to Equation 3. The dissociation rate constants were nearly independent of dGMP concentration yielding $k_{dis} = (84 \pm 4)^{-1}\ ns^{-1}$ at 20°C. The association rate constant for a dGMP concentration of 15 mM was measured to be $k_{as} = (73 \pm 3)^{-1}\ ns^{-1}$ at 20°C. Dividing the association rate constant by the dGMP concentration yields a normalized association rate constant of $(1.02 \pm 0.04) \times 10^9\ M^{-1}\ s^{-1}$, which is smaller by a factor of ~4 than the diffusion-limited bimolecular collision rate $k_{col} = (4.1 \pm 1.8) \times 10^9\ M^{-1}\ s^{-1}$. This implies that complex formation efficiency of MR121 and dGMP is on the order of 0.25 ± 0.12, or with other words, every fourth collision between freely diffusing MR121 and dGMP molecules is successful in the formation of a non-fluorescent complex.

The dissociation rate directly reflects the binding strength of MR121–dGMP complexes and follows an Arrhenius temperature dependence $k_{dis} = A \cdot \exp(-\Delta H^{dis}/k_B T)$ with dissociation enthalpy ΔH^{dis}. Figure 1c represents Arrhenius plots of association and dissociation rate constants at temperatures ranging from 10 to 40°C and a dGMP concentration of 15 mM. We found a dissociation enthalpy $\Delta H^{dis} = 31 \pm 2\ kJ\ mol^{-1}$ reflecting the binding energy of the complex, and an association enthalpy $\Delta H^{as} = 17 \pm 2\ kJ\ mol^{-1}$ which is in good agreement with the activation energy for solvent viscous flow in water [~17 kJ mol^{-1} (49)].

DNA hairpin kinetics

Having established a tool to probe contact formation between two moieties in an oligonucleotide, we will now address the main focus of this work: how does the introduction of complementary bases that can form a stem influence hairpin-loop formation in short oligonucleotides? We investigated various stem–loop structures with loops built from polythymines(dT) and stems built from pairs of the complementary nucleobases cytosine (dC, added to the 5′ end) and guanosine (dG, added to the 3′ end): F-$(dC)_y$–$(dT)_x$–$(dG)_y$, where $x = (3–9)$, $y = (1,2)$, and F is the fluorophore MR121. Intramolecular interactions between dG and MR121 that result in formation of non-fluorescent complexes were monitored using steady-state and time-resolved fluorescence as well as FCS. Measurement of kinetics of larger hairpins was limited by the signal to noise ratio of the observed quenching interaction.

Steady-state and time-resolved fluorescence spectroscopy. As seen for intermolecular quenching interactions between MR121 and dGMP, the absorption and emission spectra of DNA hairpins showed bathochromic shifts of a few nanometers compared with spectra of the free fluorophore, indicating the formation of non-fluorescent or weakly-fluorescent complexes. Comparison of relative fluorescence quantum yields of the various oligonucleotides revealed a marked influence of dC–dG pairs on loop closure (Table 1). Whereas increasing the number of dT in the loop increases the QY_{ss}, the addition of dC–dG pairs for identical loop length led to decreased QY_{ss}. All QYs were determined relative to F-$(dT)_4$ where no quencher dG is present. The observed QY_{ss} was much lower than QY_{dyn} for all hairpin samples, indicating that steady-state fluorescence is mostly affected by a static quenching interaction through formation of non-fluorescent complexes, similar to the bimolecular quenching interaction discussed above. PET that results in static quenching is much faster than the temporal resolution of our time-resolved fluorescence apparatus (~50 ps) (50,51) and can therefore not be resolved. The static quantum yield was found to resemble the population of open (fluorescent) hairpins, which can be directly observed from kinetic measurements using FCS as will be discussed in the following.

Fluorescence correlation spectroscopy. Under the assumption that MR121 and dG form non-fluorescent complexes resulting in a fluorescence signal that fluctuates between on and off states (as described above), hairpin closing can be treated as a two-state system with open (fluorescent) configuration

Table 1. DNA hairpin kinetics

Oligonucleotide	$\bar{\beta}$	$k_{op}(10^6\ s^{-1})$	ΔH_{op}(kJ mol^{-1})	I_{op}	$k_{cl}(10^6\ s^{-1})$	ΔH_{cl}(kJ mol^{-1})	I_{cl}	QY_{static}	QY_{dyn}
F-dT$_3$dG$_1$	1.00	8.42 ± 0.51	28 ± 1	28 ± 1	3.55 ± 0.31	19 ± 2	23 ± 1	0.69	0.89
F-dC$_1$dT$_3$dG$_1$	0.45 ± 0.03	0.37 ± 0.04	41 ± 3	29 ± 1	0.40 ± 0.06	30 ± 1	25 ± 1	0.43	0.83
F-dC$_2$dT$_3$dG$_2$	0.39 ± 0.02	0.35 ± 0.04	13 ± 4	18 ± 1	0.40 ± 0.04	26 ± 2	23 ± 1	0.32	0.53
F-dT$_4$dG$_1$	1.00	6.81 ± 1.03	37 ± 2	31 ± 1	2.21 ± 0.31	29 ± 3	26 ± 1	0.75	0.93
F-dC$_1$dT$_4$dG$_1$	0.47 ± 0.03	0.47 ± 0.05	43 ± 3	31 ± 1	0.41 ± 0.04	29 ± 6	25 ± 3	0.49	0.90
F-dC$_2$dT$_4$dG$_2$	0.40 ± 0.02	0.18 ± 0.02	25 ± 4	22 ± 2	0.28 ± 0.04	34 ± 2	26 ± 1	0.28	0.58
F-dT$_5$dG$_1$	1.00	5.88 ± 0.89	36 ± 6	30 ± 2	1.73 ± 0.43	28 ± 10	26 ± 4	0.79	0.97
F-dC$_1$dT$_5$dG$_1$	0.47 ± 0.07	0.70 ± 0.10	51 ± 6	35 ± 2	0.49 ± 0.03	38 ± 7	28 ± 1	0.58	0.96
F-dC$_2$dT$_5$dG$_2$	0.39 ± 0.01	0.07 ± 0.01	47 ± 2	32 ± 1	0.13 ± 0.01	46 ± 1	32 ± 1	0.27	0.75
F-dT$_6$dG$_1$	1.00	5.12 ± 0.24	33 ± 2	29 ± 1	1.36 ± 0.08	21 ± 1	23 ± 1	0.84	1.00
F-dC$_1$dT$_6$dG$_1$	0.43 ± 0.08	0.86 ± 0.02	59 ± 9	39 ± 4	0.52 ± 0.13	50 ± 11	35 ± 5	0.70	1.01
F-dC$_2$dT$_6$dG$_2$	0.38 ± 0.04	0.06 ± 0.02	48 ± 2	32 ± 1	0.09 ± 0.02	43 ± 5	30 ± 2	0.35	0.86
F-dT$_9$dG$_1$	1.00	3.30 ± 0.19	35 ± 2	29 ± 1	0.62 ± 0.02	19 ± 2	21 ± 1	0.92	1.06
F-dC$_1$dT$_9$dG$_1$	0.36 ± 0.05	0.36 ± 0.03	43 ± 2	30 ± 1	0.17 ± 0.01	24 ± 4	22 ± 2	0.83	1.07
F-dC$_2$dT$_9$dG$_2$	0.40 ± 0.03	0.06 ± 0.01	58 ± 2	35 ± 1	0.04 ± 0.01	40 ± 2	27 ± 1	0.58	1.06

Rate constants and QY were measured at 20°C. All errors represent STD.

O and closed (non-fluorescent) configuration C. FCS allows analyzing the equilibrium distribution as well as directly monitoring opening and closing rate constants $k_{cl/op}$:

$$O \underset{k_{op}}{\overset{k_{cl}}{\rightleftharpoons}} C. \qquad \mathbf{11}$$

When performing FCS measurements on the above described oligonucleotides, we found that all investigated samples display correlation curves similar to those shown in Figure 2b. All data display a fast decay occurring on a microsecond time scale, and a millisecond decay corresponding to the molecules' diffusion through the confocal excitation/detection volume.

When measuring the correlation curves of pure MR121 or oligonucleotides without dG no fluctuation components in the microsecond range were found. In order to exclude photophysical influences, such as intersystem crossing that results in population of triplet states (52), we performed FCS measurements at different excitation powers (Supplementary Data). For pure MR121 and MR121-labeled oligonucleotides submicrosecond fluctuations that can be attributed to intersystem crossing only become significant above 500 μW excitation power. Therefore, all FCS measurements were carried out at excitation powers below 500 μW in order to avoid complexity in FCS analysis due to triplet-state formation.

Figure 2b shows typical FCS curves recorded for F-(dT)$_x$–dG and F-(dC)$_y$–(dT)$_x$–(dG)$_y$ with $x = 5$ and $y = 1,2$. The data reflect fluorescence fluctuations on the microsecond time scale caused by quenching of MR121 upon contact with dG mediated by conformational dynamics of the oligonucleotides. The time scale of fluctuations that we attribute to conformational changes was in all cases well separated from that of translational diffusion. FCS curves were fitted using Equations 3 and 4 and $k_{cl/op}$ were derived following Equations 5 and 6.

Whereas data for oligonucleotides without complementary base pairs could be well described by a monoexponential decay, the introduction of a stem with as few as one dC–dG pair altered the decay significantly into a non-exponential function (for residuals see Supplementary Data). Successful fitting thus required the introduction of a

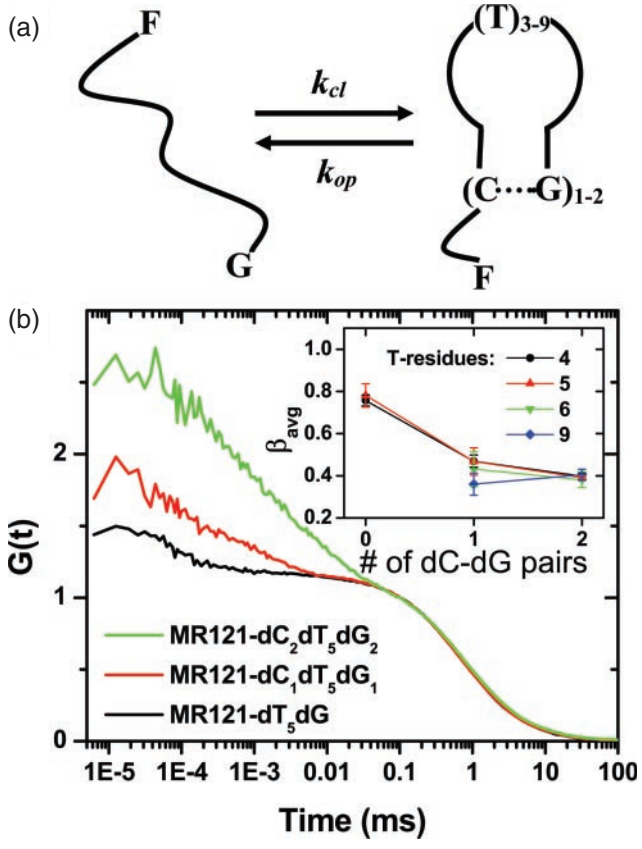

Figure 2. FCS performed on DNA hairpin structures labeled with MR121 (F). (**a**) Schematic representation of conformational fluctuations of F-labeled DNA hairpin structures. MR121 is attached at the 5′ end and connected via a loop of polythymines·(dT) to the intrinsic quencher guanosine·(dG). The stem consists of 1 or 2 cytosine (dC, incorporated at the 5′ end) and dG (incorporated at the 3′ end) pairs. (**b**) Representative FCS data shown for F-(dT)$_x$–dG (lower curve) and F-(dC)$_y$–(dT)$_x$–(dG)$_y$ with $x = 5$ and $y = 1$ (middle curve) or $y = 2$ (upper curve), where x is the number of loop bases and y the number of dC–dG pairs. Whereas FCS data for oligonucleotides without dC–dG pairs are well described by an exponential decay, those with dC–dG pairs can only be fitted with comparable accuracy using a stretched-exponential function (Equation 4). Stretch-exponents β, averaged over multiple measurements, are independent of temperature and presented as a function of dC–dG pairs with loop length x ranging from 4 to 9 (inset).

stretched-exponential function (Equation 4). We assume that the hairpin dynamics can still be described as a two-state conformational fluctuation with open and closed states (Equation 11). Stretched-exponential decays have been shown to be consistent with both static and dynamic disorder (31,47,53), where static disorder involves a number of pathways connecting open and closed hairpin states through multiple transition rates, and dynamic disorder exhibits temporal changes of transition rates. In any case, τ_{rel} corresponds to an effective relaxation time associated with the correlated motion, and β is a stretch parameter describing the heterogeneity of the system. The smaller the stretch parameter β, the broader is the distribution of transition rate constants involved.

Our data show that upon addition of a single complementary base pair, the observed relaxation decays change from mono- to stretched-exponential behavior, as reflected in the fit parameter β, which exhibits a jump from 0.8–1.0 (for oligonucleotides with no dC–dG pair) to 0.45 (for oligonucleotides with one dC–dG pair) and 0.38 (for oligonucleotides with two dC–dG pairs). A fit of equal quality was achieved for oligonucleotides without a dC–dG pair when fitting a stretched-exponential function yielding $\beta = 0.8$ or a monoexponential function with $\beta = 1.0$ (Supplementary Data).

All β-values were found to be independent of loop length and temperature. Figure 2b (inset) shows β-values for various loop lengths as a function of dC–dG pairs. Each data point is an average over nine independent measurements: three measurements at three temperatures (10–30°C). These results show that the incorporation of a stem built from one or more complementary base pairs poses the sole source of heterogeneity in observed relaxation rates.

Average closing and opening rate constants were calculated following Equation 6 and clearly show how each additional dC–dG pair leads to a slowing of opening and closing kinetics (Figure 3). Opening rate constants drop by a factor of 5–20 upon addition of a single dC residue to an oligonucleotide with a certain loop length, and the effect was the more pronounced the shorter the loop. Opening rates for F-dC–$(dT)_x$–dG with different loop lengths vary not more than a factor 3. Incorporation of a second dC–dG pair further reduces the opening rates by up to a factor of 10, but now with an inverse dependence on loop length (Figure 3a). In fact for the shortest loops with $x = 3$ there was almost no reduction of opening rates found at 20°C. Almost identical behavior was found for closing rate constants, only that relative changes were slightly smaller (Figure 3b).

When looking at relative populations of open and closed hairpins, the role of loop length becomes more obvious. We calculated the relative population of the open state $P_{open} = [O]/([O]+[C])$from the FCS amplitude $K = [C]/[O]$, where [C] and [O] are the concentrations of molecules in the open and closed configuration, respectively:

$$P_{open} = (1 + K)^{-1}. \quad \textbf{12}$$

In Figure 4 P_{open} is shown for all oligonucleotides at 10, 20 and 30°C. It appears that the influence of a single dC–dG pair on P_{open} does not change with temperature and is only slightly dependent on loop length. Addition of a second dC–dG pair, however, drives the hairpin further into the closed conformation, especially for longer loop lengths and at higher temperatures. For the long loops with >5 bases we found the reduction of P_{open} to be almost independent of temperature. For hairpins with small loops consisting of 3–4 bases and to a certain degree for 5 bases, we found a smaller effect of the second dC–dG pair on P_{open}. In particular, the population of open states was almost unaffected by the second dC–dG pair at lower temperature (Figure 4).

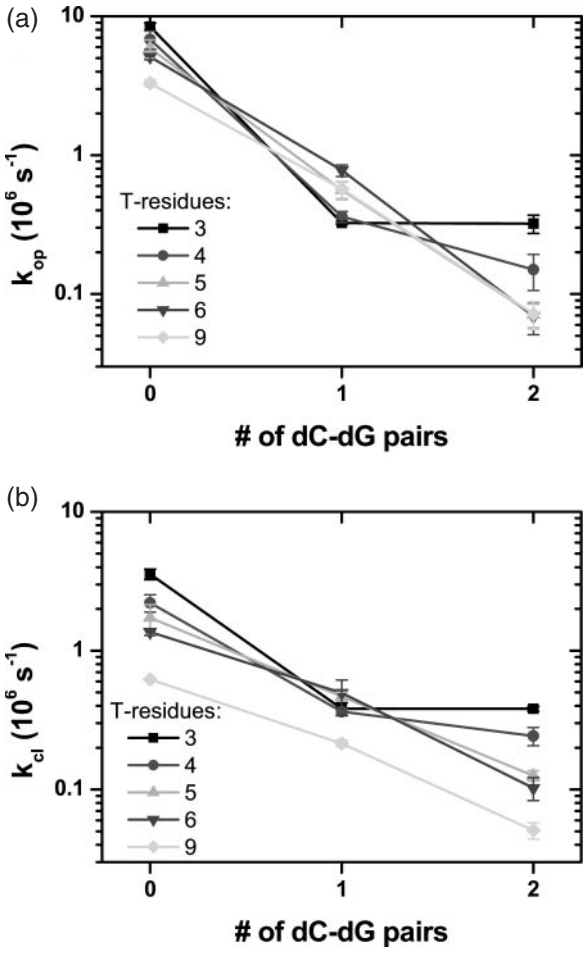

Figure 3. Opening (**a**) and closing (**b**) rate constants for F-$(dT)_x$–dG and F-$(dC)_y$–$(dT)_x$–$(dG)_y$ oligonucleotides (x ranging from 3 to 9) as a function of dC–dG pairs (y ranging from 0 to 2). Average rate constants are calculated from stretched-exponential fits (according to Equation 5) to FCS data recorded at 20°C. Errors bars represent SDs.

We further monitored kinetics of all samples at different temperatures in the range of 10–60°C. Temperature-dependent rate constants confirm the abnormal behavior found for hairpins with fewer than 5 bases in the loop: when extracting closing and opening rates from the fit parameters we found Arrhenius dependence for all samples except those with a loop of $x = 3,4$ and two dC–dG pairs. Figure 5a shows the non-Arrhenius behavior for opening rates of F-$(dC)_2$–$(dT)_4$–$(dG)_2$. Almost identical behavior was found for F-$(dC)_2$–$(dT)_3$–$(dG)_2$. Figure 5b shows a linear Arrhenius plot for closing and opening rates of F-$(dC)_2$–$(dT)_5$–$(dG)_2$, that is similar to

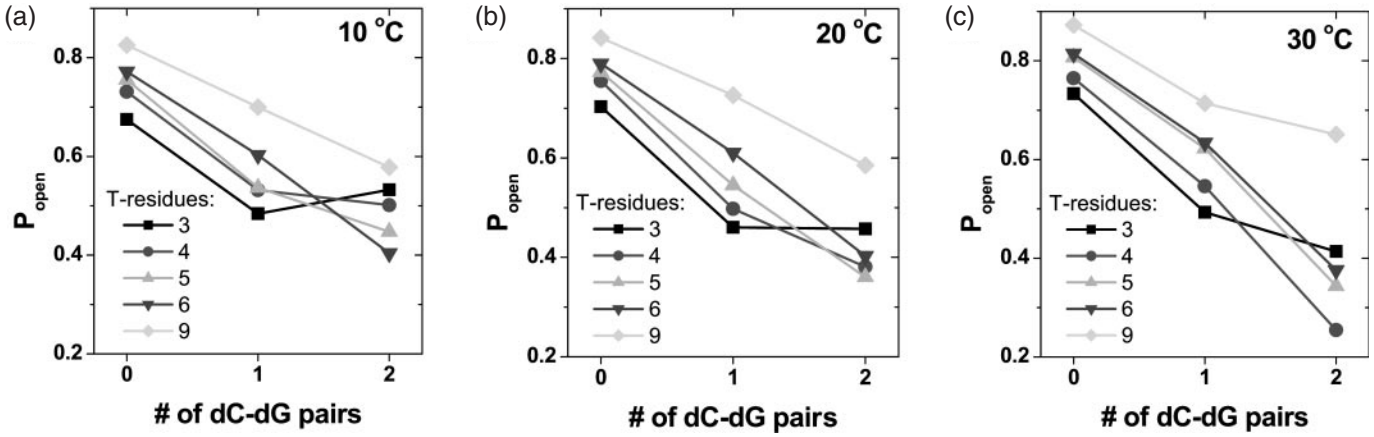

Figure 4. Population of open (that is fluorescent) states P_{open} at 10°C (**a**), 20°C (**b**) and 30°C (**c**). P_{open} is derived from rate constants measured by FCS (following Equation 12). Whereas addition of the first dC–dG pair significantly reduces P_{open} for all hairpins, the effect of a second dC–dG pair depends strongly on the loop length: for hairpins with loops longer than five residues, P_{open} is further reduced; for structures with loops of 3, 4 and 5 residues, the effect of the second dC–dG pair is temperature dependent, showing less influence on P_{open} for shorter loops and lower temperature.

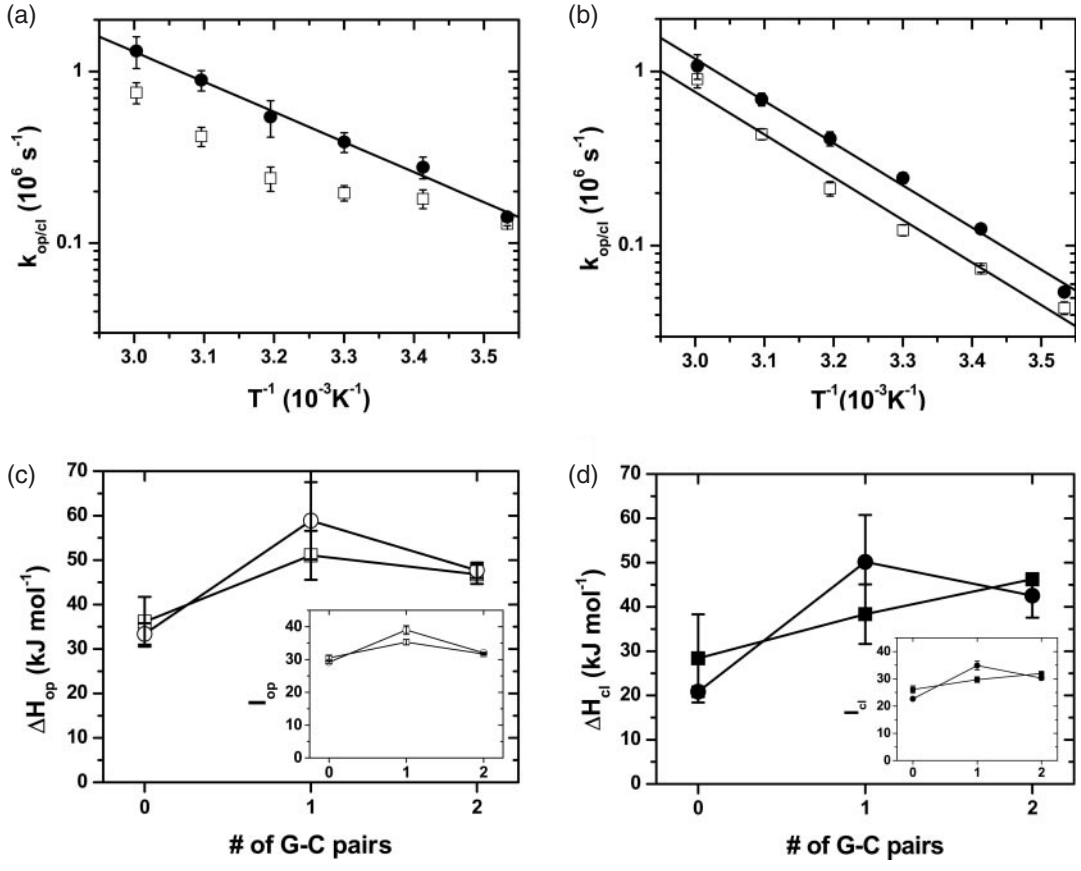

Figure 5. Arrhenius plots and activation enthalpies. Arrhenius plots of opening (open symbols) and closing (closed symbols) rate constants for (**a**) F-$(dC)_2$–$(dT)_4$–$(dG)_2$ and (**b**) F-$(dC)_2$–$(dT)_5$–$(dG)_2$ show perfect Arrhenius behavior for larger hairpins and significant deviation for those with a loop length $\leq$4. Arrhenius plots of oligonucleotides with loop length of 5 (squares) and 6 (circles) bases and 0–2 dC–dG pairs were analyzed to yield activation enthalpies and entropic contributions (insets) for the opening (**c**) and closing (**d**) process. Error bars represent SDs.

those found for all other samples. Assuming Arrhenius dependence

$$k_{op/cl} = A_{op/cl} \exp\left(- \frac{(\Delta H_{op/cl} - T\Delta S_{op/cl})}{RT} \right), \quad \textbf{13}$$

with gas constant R, temperature T, and temperature-independent entropy changes ΔS, we extracted activation enthalpies ΔH and an entropic term I, that combines ΔS and the exponential prefactor A. All parameters obtained by fitting $\ln k_{op/cl} = I_{op/cl} - \Delta H_{op/cl}(RT)^{-1}$ to

Arrhenius plots from FCS measurements are listed in Table 1.

The activation energies for dissociation of MR121–dG complexes in ssDNAs without stem are 34 ± 1 kJ mol^{-1} (S. Doose, J. Kim, H. Neuweiler and M. Sauer, manuscript in preparation) which is close to the value found for dissociation of intermolecular complexes of MR121 and dGMP (31 ± 2 kJ mol^{-1}). Noteworthy, we found no decrease in activation energy for opening with increasing loop length for ssDNAs without stem. Upon introduction of a single dC–dG pair the activation enthalpies for opening increase by ~20 kJ mol^{-1}. This value was estimated from the most reliable Arrhenius data we found for hairpins with 5 and 6 bases in the loop. Surprisingly introducing a second dC–dG pair did not result in further increase of ΔH_{op} (Figure 5c). Activation enthalpies for closing follow the same trend: they rise from a level of 20–30 kJ mol^{-1} (no dC–dG pair) by 10–30 kJ mol^{-1} when one dC–dG pair is incorporated, and remain nearly unchanged upon addition of a second dC–dG pair (Figure 5d). Furthermore we found only small changes in the entropic contribution *I* for both opening and closing process upon introduction of complementary bases (Figure 5c and d).

DISCUSSION

Opening and closing kinetics of DNA hairpins with a stem of five or more complementary base pairs have been investigated for quite some time. Puzzling results were found for the activation enthalpy of the closing process in hairpin structures, for which absorption, fluorescence quenching and FRET, investigated by FCS and T-jump methods, yielded inconsistent values (8,24,25,29). Various models have been suggested that describe possible pathways and intermediate states for the transition between the open and the closed state with correct base pairing. In this work we make an attempt to resolve the different effects that a small stem and a loop of various lengths have on hairpin dynamics. Using a well-defined and well-characterized quenching process between intrinsic guanosine residues and the oxazine fluorophore MR121, we monitored conformational dynamics of the oligonucleotide (loop) that results in end-to-end contact and subsequent hybridization of complementary base pairs located at the ends of ssDNA.

As the fluorophore F forms a complex with the dG residue that is stable on a nanosecond time scale, the interaction of F with dG contributes to the kinetics of any system where it serves as reporter. We characterized the interaction of F with dG by monitoring intermolecular complex formation between MR121 and dGMP in aqueous solution. Our results demonstrate a mechanism that is very similar to the interaction between MR121 and the amino acid tryptophan (37,38,54). The concentration dependences of dynamic and static quenching suggest that complexes are formed based on short-ranging forces, most likely of hydrophobic nature. Consistent with MD simulations for MR121 and Trp, those forces are significant for distances between fluorophore and quencher on the order of van der Waals radii, typically <1 nm (55). Even though we find slight differences in complex formation of F and dGMP compared with F and Trp with regard to association, dissociation rates and complex formation efficiency, the estimated binding energies are identical (~30 kJ mol^{-1}). The difference in association rates is reasonable, since dGMP is less accessible for the fluorophore due to steric hindrance of the attached sugar moiety. A more accurate comparison by monitoring the interaction between MR121 and guanine (i.e. without the sugar and phosphate moiety) was not possible due to poor solubility of guanine in aqueous solution.

When labeling short dG-containing poly(dT) oligonucleotides (F-(dT)$_x$–dG) with the fluorophore MR121 an intramolecular interaction between F and dG can be observed that is similar in nature to the intermolecular interaction, but mediated by DNA conformational dynamics (S. Doose, J. Kim, H. Neuweiler and M. Sauer, manuscript in preparation). Since the interaction of F with dG is based on short-ranging forces, the closing process is entirely determined by the connecting polymer and thus directly reflects conformational dynamics of the oligopyrimidine. Here it has to be pointed out that conformational dynamics of ssDNA are influenced by nucleotide interactions, such as base stacking, base pairing, and electrostatic repulsion. Once a complex is formed the binding energy of F and dG must be overcome to dissociate the complex and release the DNA termini. This is indeed confirmed by an activation enthalpy for the opening process that is only slightly larger than the binding energy of free F and dGMP (34 ± 1 kJ mol^{-1} versus 31 ± 2 kJ mol^{-1}) (S. Doose, J. Kim, H. Neuweiler and M. Sauer, manuscript in preparation). These observations suggest that measured closing kinetics for hairpin structures are unaffected by the F–dG interaction, and that the opening kinetics are always affected in the same way independent of loop and stem length.

It is further important to consider the molecular linker that connects fluorophore and oligonucleotide. MR121 is attached via its C4 carboxyl group (butyric acid) to oligonucleotides modified with a 5′-amino modifier C3 resulting in six C–C single bonds. Free rotation around aliphatic C–C bonds allows the fluorophore to occupy a certain conformational space, thus defining an effective reaction radius for the quenching interaction. We estimated a reaction radius from the molecular structure of somewhat below 1 nm. Since the unit length of one base in poly(dT) is ~0.6 nm [distance between adjacent phosphorus atoms (56)], the polymer's contour length is larger than the reaction radius for oligonucleotides with >2 bases. Since all investigated oligonucleotides consist of 4 or more bases, the prerequisite of a reaction radius that is smaller than the polymer's contour length holds.

In the following discussion, the focus will be on the striking difference of quenching kinetics for oligonucleotides with and without a complementary base pair incorporated. Steady-state fluorescence and FCS both reveal that a short oligonucleotide with one complementary base pair as stem populates stable conformations in which the fluorophore and guanine moiety can form quenched complexes. The difference to an oligonucleotide without complementary base pairs lies in added stability of the closed state (as indicated by a reduced QY), reduced opening and closing rate constants, and increased activation enthalpies for both opening and closing process (Table 1).

Since a true two-state system with constant transition rates will always result in exponential kinetics, the observation of non-exponential kinetics, as found for all hairpins in this study, reveals a distribution of rate constants, that is either static

(multiple states connected by various transition rates) or dynamic (the rate constants change over time) (31,47,53). Without having access to the accurate distribution of rate constants, our finding of non-exponential decays for stem-forming oligonucleotides implies that multiple pathways between fluorescent and non-fluorescent conformations must exist. The simple model of a static system with one fluorescent and one non-fluorescent state connected by a single pathway is only valid for ssDNA without any complementary base pair. The β-value extracted from a stretched-exponential fit is a measure for the width of the distribution and equals 0.8–1.0 in the case of monoexponential kinetics. It shows that the mere introduction of a single dC–dG pair is sufficient to broaden the distribution of transition rates significantly ($\beta = 0.45$) and that addition of a second dC–dG pair only has a small effect on further broadening ($\beta = 0.35$). No influence on the rate distribution was found for loop length and temperature changes. The β-values measured for one or two dC–dG pairs are very close to β-values that were found for hairpins with 5 complementary base pairs ($\beta = 0.44$–0.54) (30) further indicating that the distribution of rate constants is independent of stem and loop length. Our data confirm the observation that DNA hairpins fold with non-exponential folding kinetics as reported by Wallace *et al*. (30), but remain contrary to observations of exponential kinetics by Bonnet *et al*. and Ansari *et al*. (23,25). The observed distribution of transition rates could be due to a transition state ensemble, with various states representing misfolded hairpin-loops. Such a configurational diffusion model, in which mismatches in the stem are explored before the correct nucleating loop induces complete zipping of the stem, was suggested by Ansari and co-workers (25). Our data, however, demonstrate that a single dC–dG pair is sufficient to induce multiple transition states. Therefore, the transition state ensemble can not be caused solely by mismatches in the stem but interactions between stem and loop nucleotides have to be considered, too.

Taking a close look at absolute rate constants, we find a strong dependence of both opening and closing rate constants on stem size. Loop length does also influence rate constants but to a much smaller degree. Considering that the efficiency for formation of non-fluorescent complexes between free MR121 and dGMP in aqueous solution is ∼25%, the reported closing rate constants might underestimate real contact rates by a factor of ∼4. However, due to the fact that the observed time scales for hairpin folding are 1–2 orders of magnitude slower than those for bimolecular complex formation, it is reasonable that complexes are formed with nearly 100% efficiency upon mutual approach of fluorophore and quencher during hairpin closure.

In any case we observe closing rate constants on the order of 10^6 s^{-1} for one dC–dG pair. An additional dC–dG pair reduces rate constants for closing by a factor of 3–5. When simply extrapolating this result to 5 bp in the stem, we find an expected rate constant of 10^3–10^4 s^{-1}. These values are similar to rate constants observed by Wallace *et al*. and Goddard *et al*. for GGGTT–$(dA)_{30}$–AACCC hairpin structures (24,29). Considering that both the exchange of dT with dA and the length of the loop should decrease the closing rate considerably, our estimate turns out to be few orders of magnitude smaller than what has been observed. This very crude estimate suggests that the influence of added complementary base pairs on the closing rate constant is reduced with each additional base pair. Our data already show that introduction of the first complementary base pair has by far the strongest effect.

For a bimolecular interaction, as discussed above, it is obvious that the activation enthalpy of dissociation reflects the binding energy of the two compounds if entropy changes can be neglected: the free energy landscape has a global minimum for the bound state and approaches a plateau for the dissociated state. As long as roughness in the energy landscape originating from solvent viscosity [∼17 kJ mol^{-1} (49)] is small compared with the energy differences for complex formation, the binding energy can readily be derived from Arrhenius plots. When investigating hairpin-loop formation, a similar situation arises if (and only if) no transition states with higher free energy exist on the pathway between open and closed configuration.

However, the measured activation enthalpies for closing and opening of hairpins indicate that a transition state of higher enthalpy is induced by the presence of one or two dC–dG pairs as stem. It has to be pointed out that we observe positive activation enthalpies for all closing and opening processes in all investigated samples, since some controversy arouse from previous reports of negative and positive activation enthalpies for larger hairpins (28,29). Only recently did Jung and vanOrden (8) suggest a three-state mechanism which could resolve the debate about activation enthalpies in favor of our presented analysis. Our results argue for positive closing and opening activation enthalpies that depend on the presence of dC–dG pairs but are independent of the number of pairs. In fact there is surprising agreement between the activation enthalpy for opening found in this work and found by Wallace *et al*. (29) for GGGTT–$(dA)_{30}$–AACCC (59 kJ mol^{-1}), which also points to rather small contributions of additional complementary base pairs to the overall activation enthalpy for opening. It is interesting to note that there is a striking difference in behavior between opening rate constants and activation enthalpies for the addition of the second dC–dG pair. Whereas both opening and closing rate constants decrease by the same amount as observed upon addition of the first dC–dG pair, the activation enthalpies remain nearly unchanged.

The described effects were consistently observed for hairpin structures with a loop length longer than 4 bases. For hairpins with loop length of 3–4, and below room temperature for 5 bases, we found a smaller effect on the opening rate constant when incorporating a second dC–dG pair. The deviation from the expected behavior depends on temperature, which is also reflected in non-linear Arrhenius plots. These results clearly demonstrate that intramolecular strain contributes to the closing process of hairpin structures with loop length <5 bases. This is in agreement with previous investigations which suggested that in small DNA hairpin-loops bases of the stem are broken apart to maintain an optimal loop size of 4–5 bases (13).

CONCLUSION

We demonstrated that PET between an extrinsic fluorophore (the oxazine derivative MR121) and an intrinsic guanosine

residue in combination with FCS (PET-FCS) can be used to monitor conformational dynamics in small DNA structures. The method allows directly monitoring opening and closing rate constants in DNA hairpins in thermodynamic equilibrium with high sensitivity and a temporal resolution down to nanoseconds.

We first characterized the formation of non-fluorescent complexes between freely diffusing MR121 and dGMP. The quenching interaction has similar characteristics to the previously analyzed interaction between MR121 and Trp (54). Complexes are formed upon diffusional contact with an efficiency of ~25% and a binding energy of ~30 kJ mol^{-1}. Monitoring intramolecular quenching interactions in oligonucleotides, we resolved that one complementary base pair adds significant stability to the closed state. At the same time the opening and closing rates drop by a factor of 5–20 and the activation enthalpies increase. Adding a second complementary base pair to the stem structure further decreases opening and closing rate constants, however, without significantly changing activation enthalpies. All investigated samples exhibit positive activation enthalpies above the level for viscous drag in aqueous solution and above the level for end-to-end kinetics in ssDNA. All measured kinetics for DNA hairpins with a stem of one or more base pairs exhibit multiexponential decays contrary to end-to-end kinetics in ssDNA. Our results thus highlight the importance of a single pair of complementary DNA bases for the initial step of DNA hairpin folding. They further imply that the time scale for hairpin folding is strongly influenced by interactions between stem and loop nucleotides. These interactions, most likely due to base stacking or transient base pairing, are stronger between dC and dT than between dT and dT.

The use of PET-FCS extends experimental knowledge of hairpin dynamics to length scales inaccessible for FRET measurements. The method has proven to be useful for monitoring dynamics on length scales below ~3 nm, a length scale that is hardly accessible by FRET experiments, in a number of DNA structures. Application to nucleotide-based nanostructures provides new means to directly observe hybridization events, conformational changes and possibly investigate DNA machines at work.

SUPPLEMENTARY DATA

Supplementary Data are available at NAR Online.

ACKNOWLEDGEMENTS

We thank K. H. Drexhage for providing the oxazine derivative MR121. We are grateful to Gerd Wiebusch and Stefan Wörmer for technical assistance. Research described in this article was supported by the BMBF (grant no. 13N8349), and the DFG (grant no. SFB 613). J.K. was supported by the Korea Research Foundation Grant funded by the Korean Government (MOEHRD, Basic Research Promotion Fund M01-2004-000-10234-0). Funding to pay the Open Access publication charges for this article was provided by the DFG (grant no. SFB 613).

Conflict of interest statement. None declared.

REFERENCES

1. Varani,G. (1995) Exceptionally stable nucleic acid hairpins. *Annu. Rev. Biophys. Biomol. Struct.*, **24**, 379–404.
2. Uhlenbeck,O.C. (1990) Tetraloops and RNA folding. *Nature*, **346**, 613–614.
3. Tyagi,S. and Kramer,F.R. (1996) Molecular beacons: probes that fluoresce upon hybridization. *Nat. Biotechnol.*, **14**, 303–308.
4. Kostrikis,L.G., Tyagi,S., Mhlanga,M.M., Ho,D.D. and Kramer,R.F. (1998) Molecular beacons: spectral genotyping of human alleles. *Science*, **279**, 1228–1229.
5. Bonnet,G., Tyagi,S., Libchaber,A. and Kramer,F.R. (1999) Thermodynamic basis of the enhanced specificity of structured DNA probes. *Proc. Natl Acad. Sci. USA*, **96**, 6171–6176.
6. Ansari,A. and Kuznetsov,S.V. (2005) Is hairpin formation in single-stranded polynucleotide diffusion-controlled? *J. Phys. Chem. B*, **109**, 12982–12989.
7. Wang,X. and Nau,W.M. (2004) Kinetics of end-to-end collision in short single-stranded nucleic acids. *J. Am. Chem. Soc.*, **126**, 808–813.
8. Jung,J. and VanOrden,A. (2006) A three-state mechanism for dna hairpin folding characterized by multiparameter fluorescence fluctuation spectroscopy. *J. Am. Chem. Soc.*, **128**, 1240–1249.
9. Elson,E.L., Scheffler,I.E. and Baldwin,R.L. (1970) Helix formation by d(TA) oligomers. 3. Electrostatic effects. *J. Mol. Biol.*, **54**, 401–415.
10. Gralla,J. and Crothers,D.M. (1973) Free energy of imperfect nucleic acid helices. II. Small hairpin loops. *J. Mol. Biol.*, **73**, 497–511.
11. Uhlenbeck,O.C., Borer,P.N., Dengler,B. and Tinoco,I.Jr (1973) Stability of RNA hairpin loops: A6-Cm-U6. *J. Mol. Biol.*, **73**, 483–496.
12. Haasnoot,C.A., Hilbers,C.W., van der Marel,G.A., van Boom,J.H., Singh,U.C., Pattabiraman,N. and Kollman,P.A. (1986) On loop folding in nucleic acid hairpin-type structures. *J. Biomol. Struct. Dyn.*, **3**, 843–857.
13. Hilbers,C.W., Haasnoot,C.A., de Bruin,S.H., Joordens,J.J., van der Marel,G.A. and van Boom,J.H. (1985) Hairpin formation in synthetic oligonucleotides. *Biochimie*, **67**, 685–695.
14. Wemmer,D.E., Chou,S.H., Hare,D.R. and Reid,B.R. (1985) Duplex-hairpin transitions in DNA: NMR studies on CGCGTATACGCG. *Nucleic Acids Res.*, **13**, 3755–3772.
15. Senior,M.M., Jones,R.A. and Breslauer,K.J. (1988) Influence of loop residues on the relative stabilities of DNA hairpin structures. *Proc. Natl Acad. Sci. USA*, **85**, 6242–6246.
16. Zuker,M. (1989) On finding all suboptimal foldings of an RNA molecule. *Science*, **244**, 48–52.
17. Paner,T.M., Amaratunga,M., Doktycz,M.J. and Benight,A.S. (1990) Analysis of melting transitions of the DNA hairpins formed from the oligomer sequences d[GGATAC(X)4GTATCC] (X = A, T, G, C). *Biopolymers*, **29**, 1715–1734.
18. Vallone,P.M., Paner,T.M., Hilario,J., Lane,M.J., Faldasz,B.D. and Benight,A.S. (1999) Melting studies of short DNA hairpins: influence of loop sequence and adjoining base pair identity on hairpin thermodynamic stability. *Biopolymers*, **50**, 425–442.
19. Rentzeperis,D., Alessi,K. and Marky,L.A. (1993) Thermodynamics of DNA hairpins: contribution of loop size to hairpin stability and ethidium binding. *Nucleic Acids Res.*, **21**, 2683–2689.
20. Serra,M.J., Axenson,T.J. and Turner,D.H. (1994) A model for the stabilities of RNA hairpins based on a study of the sequence dependence of stability for hairpins of six nucleotides. *Biochemistry*, **33**, 14289–14296.
21. Hirao,I., Kawai,G., Yoshizawa,S., Nishimura,Y., Ishido,Y., Watanabe,K. and Miura,K. (1994) Most compact hairpin-turn structure exerted by a short DNA fragment, d(GCGAAGC) in solution: an extraordinarily stable structure resistant to nucleases and heat. *Nucleic Acids Res.*, **22**, 576–582.
22. Ma,H., Proctor,D.J., Kierzek,E., Kierzek,R., Bevilacqua,P.C. and Gruebele,M. (2006) Exploring the energy landscape of a small RNA hairpin. *J. Am. Chem. Soc.*, **128**, 1523–1530.
23. Bonnet,G., Krichevsky,O. and Libchaber,A. (1998) Kinetics of conformal fluctuations in DNA hairpin loops. *Proc. Natl Acad. Sci. USA*, **95**, 8602–8606.
24. Goddard,N.L., Bonnet,G., Krichevsky,O. and Libchaber,A. (2000) Sequence dependent rigidity of single stranded DNA. *Phys. Rev. Lett.*, **85**, 2400–2403.

25. Ansari,A., Kuznetsov,S.V. and Shen,Y. (2001) Configurational diffusion down a folding funnel describes the dynamics of DNA hairpins. *Proc. Natl Acad. Sci. USA*, **98**, 7771–7776.
26. Ansari,A., Shen,Y. and Kuznetsov,S.V. (2002) Misfolded loops decrease the effective rate of DNA hairpin formation. *Phys. Rev. Lett.*, **88**, 069801.
27. Shen,Y.Q., Kuznetsov,S.V. and Ansari,A. (2001) Loop dependence of the dynamics of DNA hairpins. *J. Phys. Chem. B*, **105**, 12202–12211.
28. Kuznetsov,S.V., Shen,Y., Benight,A.S. and Ansari,A. (2001) A semiflexible polymer model applied to loop formation in DNA hairpins. *Biophys. J.*, **81**, 2864–2875.
29. Wallace,M.I., Ying,L., Balasubramanian,S. and Klenerman,D. (2001) Non-Arrhenius kinetics for the loop closure of a DNA hairpin. *Proc. Natl Acad. Sci. USA*, **98**, 5584–5589.
30. Wallace,M.I., Ying,L.M., Balasubramanian,S. and Klenerman,D. (2000) FRET fluctuation spectroscopy: exploring the conformational dynamics of a DNA hairpin loop. *J. Phys. Chem. B*, **104**, 11551–11555.
31. Ying,L.M., Wallace,M.I. and Klenerman,D. (2001) Two-state model of conformational fluctuation in a DNA hairpin-loop. *Chem. Phys. Lett.*, **334**, 145–150.
32. Heinlein,T., Knemeyer,J.P., Piestert,O. and Sauer,M. (2003) Photoinduced electron transfer between fluorescent dyes and guanosine residues in DNA-hairpins. *J. Phys. Chem. B*, **107**, 7957–7964.
33. Knemeyer,J.P., Marme,N. and Sauer,M. (2000) Probes for detection of specific DNA sequences at the single-molecule level. *Anal. Chem.*, **72**, 3717–3724.
34. Widengren,J., Dapprich,J. and Rigler,R. (1997) Fast interactions between R6G and dGTP in water studied by fluorescence correlation spectroscope. *Chem. Phys.*, **216**, 417–426.
35. Seidel,C.A.M., Schulz,A. and Sauer,M.H.M. (1996) Nucleobase-specific quenching of fluorescent dyes .1. Nucleobase one-electron redox potentials and their correlation with static and dynamic quenching efficiencies. *J. Phys. Chem. B*, **100**, 5541–5553.
36. Edman,L., Mets,U. and Rigler,R. (1996) Conformational transitions monitored for single molecules in solution. *Proc. Natl Acad. Sci. USA*, **93**, 6710–6715.
37. Neuweiler,H., Doose,S. and Sauer,M. (2005) A microscopic view of miniprotein folding: Enhanced folding efficiency through formation of an intermediate. *Proc. Natl Acad. Sci. USA*, **102**, 16650–16655.
38. Neuweiler,H. and Sauer,M. (2004) Using photoinduced charge transfer reactions to study conformational dynamics of biopolymers at the single-molecule level. *Curr. Pharm. Biotechnol.*, **5**, 285–298.
39. Piestert,O., Barsch,H., Buschmann,V., Heinlein,T., Knemeyer,J.P., Weston,K.D. and Sauer,M. (2003) A single-molecule sensitive DNA hairpin system based on intramolecular electron transfer. *Nano Letters*, **3**, 979–982.
40. Stöhr,K., Hafner,B., Nolte,O., Wolfrum,J., Sauer,M. and Herten,D.P. (2005) Species-specific identification of mycobacterial 16S rRNA PCR amplicons using smart probes. *Anal. Chem.*, **77**, 7195–7203.
41. Magde,D., Elson,E.L. and Webb,W.W. (1974) Fluorescence correlation spectroscopy. II. An experimental realization. *Biopolymers*, **13**, 29–61.
42. Rigler,R., Mets,U., Widengren,J. and Kask,P. (1993) Fluorescence correlation spectroscopy with high count rate and low background—analysis of translational diffusion. *Eur. Biophys. J.*, **22**, 169–175.
43. Li,H., Ren,X., Ying,L., Balasubramanian,S. and Klenerman,D. (2004) Measuring single-molecule nucleic acid dynamics in solution by two-color filtered ratiometric fluorescence correlation spectroscopy. *Proc. Natl Acad. Sci. USA*, **101**, 14425–14430.
44. Chattopadhyay,K., Elson,E.L. and Frieden,C. (2005) The kinetics of conformational fluctuations in an unfolded protein measured by fluorescence methods. *Proc. Natl Acad. Sci. USA*, **102**, 2385–2389.
45. Hess,S.T., Huang,S., Heikal,A.A. and Webb,W.W. (2002) Biological and chemical applications of fluorescence correlation spectroscopy: a review. *Biochemistry*, **41**, 697–705.
46. Berne,B.J. and Pecora,R. (1976) *Dynamic Light Scattering*. Wiley, NY.
47. Klafter,J. and Shlesinger,M.F. (1986) On the relationship among three theories of relaxation in disordered systems. *Proc. Natl Acad. Sci. USA*, **83**, 848–851.
48. Lakowicz,J.R. (1999) *Principles of Fluorescence Spectroscopy*. Kluwer Academic/Plenum Publishers, NY.
49. Lide,D.R. (1994) *CRC Handbook of Chemistry and Physics*. 75th edn. CRC Press, Boca Raton, FI.
50. Fiebig,T., Wan,C., Kelley,S.O., Barton,J.K. and Zewail,A.H. (1999) Femtosecond dynamics of the DNA intercalator ethidium and electron transfer with mononucleotides in water. *Proc. Natl Acad. Sci. USA*, **96**, 1187–1192.
51. Wan,C., Fiebig,T., Kelley,S.O., Treadway,C.R., Barton,J.K. and Zewail,A.H. (1999) Femtosecond dynamics of DNA-mediated electron transfer. *Proc. Natl Acad. Sci. USA*, **96**, 6014–6019.
52. Widengren,J., Mets,U. and Rigler,R. (1995) Fluorescence correlation spectroscopy of triplet states in solution—a theoretical and experimental study. *J. Phys. Chem. B*, **99**, 13368–13379.
53. Metzler,R., Klafter,J., Jortner,J. and Volk,M. (1998) Multiple time scales for dispersive kinetics in early events of peptide folding. *Chem. Phys. Lett.*, **293**, 477–484.
54. Doose,S., Neuweiler,H. and Sauer,M. (2005) A close look at fluorescence quenching of organic dyes by tryptophan. *Chem. Phys. Chem.*, **6**, 2277–2285.
55. Vaiana,A.C., Neuweiler,H., Schulz,A., Wolfrum,J., Sauer,M. and Smith,J.C. (2003) Fluorescence quenching of dyes by tryptophan: interactions at atomic detail from combination of experiment and computer simulation. *J. Am. Chem. Soc.*, **125**, 14564–14572.
56. Murphy,M.C., Rasnik,I., Cheng,W., Lohman,T.M. and Ha,T. (2004) Probing single-stranded DNA conformational flexibility using fluorescence spectroscopy. *Biophys. J.*, **86**, 2530–2537.